Neuro-Oncology

Neuro-Oncology 17(6), 784–800, 2015
doi:10.1093/neuonc/nou322
Advance Access date 27 December 2014

Current standards and new concepts in MRI and PET response assessment of antiangiogenic therapies in high-grade glioma patients

Markus Hutterer, Elke Hattingen, Christoph Palm, Martin Andreas Proescholdt, and Peter Hau

Department of Neurology and Wilhelm-Sander Neuro-Oncology Unit, University Hospital and Medical School, Regensburg, Germany (M.H., P.H.); Neuroradiology, Department of Radiology, University Hospital Bonn, Bonn, Germany (E.H.); Regensburg Medical Image Computing, Ostbayerische Technische Hochschule Regensburg, Regensburg, Germany (C.P.); Department of Neurosurgery, University Hospital and Medical School, Regensburg, Germany (M.P.)

Corresponding Author: Peter Hau, MD, Department of Neurology and Wilhelm-Sander NeuroOncology Unit, University of Regensburg Medical School, Franz Josef Strauß-Allee 11, D-93053 Regensburg, Germany (peter.hau@ukr.de).

Despite multimodal treatment, the prognosis of high-grade gliomas is grim. As tumor growth is critically dependent on new blood vessel formation, antiangiogenic treatment approaches offer an innovative treatment strategy. Bevacizumab, a humanized monoclonal antibody, has been in the spotlight of antiangiogenic approaches for several years. Currently, MRI including contrast-enhanced T1-weighted and T2/fluid-attenuated inversion recovery (FLAIR) images is routinely used to evaluate antiangiogenic treatment response (Response Assessment in Neuro-Oncology criteria). However, by restoring the blood–brain barrier, bevacizumab may reduce T1 contrast enhancement and T2/FLAIR hyperintensity, thereby obscuring the imaging-based detection of progression. The aim of this review is to highlight the recent role of imaging biomarkers from MR and PET imaging on measurement of disease progression and treatment effectiveness in antiangiogenic therapies. Based on the reviewed studies, multimodal imaging combining standard MRI with new physiological MRI techniques and metabolic PET imaging, in particular amino acid tracers, may have the ability to detect antiangiogenic drug susceptibility or resistance prior to morphological changes. As advances occur in the development of therapies that target specific biochemical or molecular pathways and alter tumor physiology in potentially predictable ways, the validation of physiological and metabolic imaging biomarkers will become increasingly important in the near future.

Keywords: high-grade glioma, antiangiogenic treatment, MRI, PET, multimodal response assessment.

High-grade gliomas (HGGs) are highly aggressive primary brain tumors. Despite multimodal treatment, patients with HGGs, in particular glioblastoma multiforme (GBM), have an unfavorable prognosis.[1] After first tumor recurrence, the median survival ranges between only 3 and 9 months.[2,3]

As tumor growth is critically dependent on new blood vessel formation, antiangiogenic treatment approaches offer an attractive treatment strategy.[4] The coincidence of pathological neovascularization and high expression levels of vascular endothelial growth factor (VEGF) led to the conception that VEGF may be a suitable target for antiangiogenic treatment.[5] Bevacizumab, a humanized monoclonal antibody targeting VEGF-A, has been in the spotlight of antiangiogenic therapies for several years. Recently, bevacizumab was investigated in 2 large-scale, randomized, phase III trials (AVAglio and RTOG-0825)[6,7] for GBM first-line treatment and demonstrated improved progression-free survival (PFS) in both trials and maintained quality of life in the AVAglio trial. Both studies failed to prolong overall survival (OS). Results from clinical trials in recurrent HGG (rHGG) reported response rates of 28%–57%, improved 6-month PFS rates of 29%–50%, decreased peritumoral edema, and improved quality of life.[3,8–11] A recently published phase II randomized trial of first recurrent GBM (rGBM) showed an improvement of the combination of bevacizumab and lomustine in comparison with bevacizumab or lomustine alone (BELOB study)[12] and led to the adaptation of the running European Organisation for Research and Treatment of Cancer 26101 study to a 2-arm randomized phase III registration trial.

Currently, contrast-enhanced MRI is routinely used to evaluate antiangiogenic treatment response.[9,10] Since contrast enhancement reflects vascular permeability, therapeutic strategies blocking VEGF and, therefore, reducing tumor vascular permeability may have a significant impact on the heavily MR-based tumor response criteria, formulated initially by

Received 3 July 2014; accepted 30 October 2014

Macdonald and colleagues[13] and later by the Response Assessment in Neuro-Oncology (RANO) working group.[14] Therefore, the validity of traditional imaging assessment of PFS has been questioned, and innovative imaging strategies are warranted.

Therefore, we provide an in-depth comprehensive analysis of current studies of baseline, early-, and late-change imaging biomarkers derived from structural and advanced MR and metabolic PET imaging following antiangiogenic treatment in HGG. In addition, we discuss key issues in imaging biomarker validation and qualification.

Standard MRI

Outcome and Response Evaluation

Currently, standard MRI, including contrast-enhanced T1-weighted images (CE-T1WI), is routinely used to evaluate antiangiogenic treatment response in clinical trials and daily neuro-oncological practice.[14] Contrast enhancement was generally considered to show vital tumor tissue, since it reflects the abnormal blood–brain barrier (BBB) permeability of the notoriously abundant dysfunctional tumor vessels of HGG. However, contrast enhancement may significantly decrease following BBB normalization by antiangiogenic agents, and this effect can occur as early as 24–48 h after initiation of therapy.[9–11] This observation is not necessarily indicative of a true antitumor effect and has, therefore, been termed a "pseudo-response."[14] Furthermore, highly infiltrative HGG tumor burden is not always associated with abnormal BBB permeability ("nonenhancing tumor"). As these tumors still yield a signal increase on T2-weighted and fluid-attenuated inversion recovery (FLAIR) images, these imaging characteristics were introduced in the revised RANO response criteria[14] together with the term "pseudo-response,"[14] which indicates a more than 50% reduction of contrast enhancement but is not associated with a significant decrease of nonenhancing tumor. However, there remain unresolved issues yet. The RANO criteria do not yet quantify the degree of T2/FLAIR changes to define tumor progression. Furthermore, tumor-related edema or ischemia, radiation-induced changes, demyelination, and infection can result in hyperintense T2/FLAIR signals, which makes it difficult to distinguish nonneoplastic signal alterations from nonenhancing tumor. Further, progression patterns under bevacizumab treatment may vary considerably among patients with HGGs, complicating the evaluation of treatment response.[15]

T1-Weighted Imaging

Each MRI protocol for brain tumor imaging includes pre- and postcontrast T1WI. The current tumor response criteria are based on 2D measurements of tumor cross-sectional areas on CE-T1WI rather than a 3D volume calculation. It has been shown that conventional 2D evaluation is comparable to 3D volume measurement.[16,17] In contrast, other studies have revealed that automatic segmentation is more sensitive for detecting tumor progression than is subjective MRI assessment.[18]

Despite the limitations of standard MRI, several studies have demonstrated that treatment response criteria,[11,19–23] pretreatment CE-T1WI tumor volumes,[24,25] early CE-T1WI tumor volume changes, and residual CE-T1WI volumes in the early follow-up MRI scans might serve as predictors for both PFS and OS (Table 1).[17,24,25] In contrast, baseline or early posttreatment T2/FLAIR volumes and T2/FLAIR volume changes were not significantly associated with improved outcome (Table 1).[17,24,25] These results indicate that the antiangiogenic effect, reflected by a reduction in contrast enhancement, might be associated with real antitumor effect and with better prognosis for the patient.

In addition, bevacizumab treatment induces response-related tumor calcification depicted as hyperintense areas on precontrast T1WI and associated with better prognosis (see also diffusion-restriction and tumor calcification below).[26,27]

T2/FLAIR Sequences

Despite the fact that changes in T2/FLAIR volume upon initial bevacizumab treatment are not a predictor for PFS and OS, the pretreatment ratio of FLAIR/contrast-enhancing volume might be predictive for both,[24] being unique features accessible before starting the bevacizumab therapy. The authors of this work argue that these results may indicate that nonenhancing tumor-related changes at recurrence are related to a better outcome. However, T2/FLAIR hyperintensities observed in HGGs delineate not only nonenhancing tumor but also tumor-associated edema, treatment-related changes (eg, perioperative ischemia, infection/inflammation, postradiation demyelination, leukencephalopathy).[28] After initiation of bevacizumab therapy, there is frequently an impressive reduction of edema leading to a decreased edema/tumor volume ratio and reduced necrotic tumor areas.[18,29,30] Since tumor infiltration is associated with less edema under bevacizumab therapy, T2/FLAIR imaging may more appropriately show tumor infiltration. However, the high signal in T2/FLAIR images is physically based on a prolongation of the T2-relaxation time compared with normal tissue, which is less pronounced during bevacizumab treatment compared with pretreatment.[31] This leads to a specific change of the T2/FLAIR signal of the tumor,[30] resulting in a low reliability of T2/FLAIR evaluation with a high interobserver variability.[32]

One approach to better detect nonenhancing tumors is to subtract T2-relaxation-time maps during bevacizumab treatment from the map of best response (first scan after treatment started), so that even subtle changes may be detectable.[31,33] Artzi et al[34] recently reported another approach identifying nonenhancing FLAIR areas as tumor using multiple MRI parameters based on mean diffusivity and fractional anisotropy, cerebral blood volume (CBV), and flow maps. An increase of the percentage of the tumor-infiltrative volume detected at weeks 8 and 16 but not at baseline was associated with poorer PFS (Table 1).

Advanced MRI

Diffusion-Weighted Imaging

Diffusion-weighted imaging (DWI) was introduced in tumor diagnosis as a method indicating cell density of a tumor. The underlying rationale came from stroke imaging: narrowed extracellular space decreases the diffusion of water molecules

Table 1. Standard MRI biomarker

Modality	Imaging Biomarker	Time Point	Outcome Measure			Improved PFS	Improved OS	Ref.
Response assessment	*Macdonald*	Early-BEV	4 w scan	**CR/PR**	17/48 (35%) rGBM pts	$P = .070$[(a)]	N/A	11
			8 w scan	**CR/PR**	11/32 (34%) rGBM pts	**$P = .004$**[(a)]	N/A	19
	Levin	Early-BEV	96 h scan	**CR/PR**	42/48 (87%) rGBM pts	**$P < .001$**[(a)]	N/A	11
			4 w scan	**CR/PR**	34/48 (71%) rGBM pts	**$P = .030$**[(a)]	N/A	
	Revised Macdonald, RANO criteria	Early-BEV	6 w scan	**CR/PR**	20/33 (61%) rAG pts	$P = .090$[(c)]	$P = .100$[(c)]	20
			N/A	**CR/PR**	12/25 (48%) rGBM pts	**$P = .003$**[(a)]	$P = .290$[(a)]	21
			N/A	**CR/PR**	10/32 (31%) rAG pts	**$P = .020$**[(a)]	**$P = .020$**[(a)]	
			6 w scan	**CR/PR**	9/30 (31%) rHGG pts	**$P = .003$**[(b)], $P = .054$[(c)]	**$P = .016$**[(b)], $P = .382$[(c)]	23
		Early-BEV	9 w scan	**CR/PR**	30/157 (33%) rGBM pts	$P = .346$ (HR 0.78)[(c)]	**$P = .009$ (HR 0.52)**[(c)]	22
		Late-BEV	18 w scan	**CR/PR**	46/147 (31%) rGBM pts	$P = .326$ (HR 1.33)[(c)]	**$P = .001$ (HR 0.48)**[(c)]	
			26 w scan	**CR/PR**	51/123 (41%) rGBM pts	$P = .798$ (HR 1.14)[(c)]	**$P < .001$ (HR 0.43)**[(c)]	
T1WI	*Tumor calcification*	Early-BEV	8–16 w scan	**Tumor calcification**, 22/36 (61%) rGBM pts[(A)]		**$P < .001$**[(a)]	**$P = .006$**[(a)]	27
			N/A	**Tumor calcification**, 25/74 (34%) rGBM pts[(B)]		N/A	**$P < .001$**[(a)]	26
			N/A	**Tumor calcification + DWI restriction**, 21/74 (28%) rGBM[(B)]		N/A	**$P < .001$**[(a)]	26
CE-T1WI	*Enhancing tumor volume ($V^{CE\text{-}T1WI}$)*[1]	Baseline	Pre-BEV	**$V^{CE\text{-}T1WI}$ pre-BEV** (<5 mL to <20 mL) (84 rGBM pts)		**$P = .031$**[(a)]	$P = .060$[(a)]	24
				$V^{CE\text{-}T1WI}$ pre-BEV < median $V^{CE\text{-}T1WI}$ (15.2 mL)		$P = .065$[(a)]	**$P = .006$**[(a)]	
			Pre-BEV	**$V^{CE\text{-}T1WI}$ pre-BEV** (volumetric continuous variable) (91 rGBM pts)		**$P = .037$ (HR 1.01)**[(c)]	**$P < .001$ (HR 1.02)**[(c)]	25
				$V^{CE\text{-}T1WI}$ pre-BEV (multivariable COX analysis)		$P = .75$[(c)]	**$P = .041$ (HR 1.02)**[(c)]	
				$V^{CE\text{-}T1WI}$ pre-BEV < median $V^{CE\text{-}T1WI}$ (19.5 cm^3)[(C)]		**$P = .030$ (HR 2.40)**[(c)]	**$P = .001$ (HR 4.93)**[(c)]	
			Early-BEV	6 w scan	**$V^{CE\text{-}T1WI}$ post-BEV** (<2.5 mL to <10 mL)	**$P = .023$**[(a)]	$P = .342$[(a)]	24
					$V^{CE\text{-}T1WI}$ post-BEV change (>25% to > 75% decrease)	$P = .743$[(a)]	$P = .620$[(a)]	
					$V^{CE\text{-}T1WI}$ post-BEV < median $V^{CE\text{-}T1WI}$ (7.7 mL)	$P = .076$[(a)]	$P = .170$[(a)]	
				4–6 w scan	**$V^{CE\text{-}T1WI}$ post-BEV** (volumetric continuous variable)	**$P < .001$ (HR 1.03)**[(c)]	**$P < .001$ (HR 1.03)**[(c)]	25
					$V^{CE\text{-}T1WI}$ post-BEV (multivariable COX analysis)	**$P < .001$ (HR 1.04)**[(c)]	**$P < .001$ (HR 1.03)**[(c)]	
					$V^{CE\text{-}T1WI}$ post-BEV < median $V^{CE\text{-}T1WI}$ (7.8 cm^3)[(D)]	**$P = .036$ (HR 2.12)**[(c)]	**$P < .001$ (HR 4.37)**[(c)]	
					$V^{CE\text{-}T1WI}$ post-BEV change (volumetric continuous variable)	**$P = .001$ (HR .48)**[(c)]	**$P = .002$ (HR .56)**[(c)]	
					$V^{CE\text{-}T1WI}$ post-BEV change (≥52% decrease)[(E)]	**$P = .009$ (HR .39)**[(c)]	**$P = .013$ (HR .37)**[(c)]	
				8 w scan	**$V^{CE\text{-}T1WI}$ decrease ≥ 50%** **2D evaluation**[(F)] (107 rGBM pts)	N/A	$P = .513$[(a)]	17
					3D segmentation[(F)]	N/A	$P = .105$[(a)]	
			Late-BEV	16 w scan	**$V^{CE\text{-}T1WI}$ decrease ≥ 50%** **2D evaluation**[(F)]	N/A	$P = .888$[(a)]	17
					3D segmentation[(F)]	N/A	$P = .120$[(a)]	
T2/FLAIR	*Peritumoral edema*[(2)]	Baseline	Pre-BEV	**V^{FLAIR} pre-BEV** (<100 mL to <250 mL)		$P = .310$[(a)]	$P = .360$[(a)]	24
				V^{FLAIR} pre-BEV (volumetric continuous variable)		$P = .570$ (HR 1.00)[(c)]	$P = .150$ (HR 1.00)[(c)]	25
			Early-BEV	6 w scan	**V^{FLAIR} post-BEV** (<100 mL to <200 mL)	$P = .583$[(a)]	$P = .571$[(a)]	24
				4–6 w scan	**V^{FLAIR} post-BEV** (volumetric continuous variable)	**$P = .018$ (HR 1.01)**[(c)]	**$P = .025$ (HR 1.01)**[(c)]	25

				V^{FLAIR} post-BEV (multivariable COX analysis)	$P = .550$ (HR 1.00)[c]	$P = .051$ (HR 0.99)[c]	
			4–6 w scan	**V^{FLAIR} post-BEV change** (>25% to >50% decrease)	$P = .282$[a]	$P = .466$[a]	24
			8 w scan	**V^{FLAIR} post-BEV change** (>50% decrease)	N/A	$P = .383$[a]	17
			16 w scan	**V^{FLAIR} post-BEV change** (>50% decrease)	N/A	$P = .127$[a]	
CE-T1WI + T2/FLAIR	*rNTR*[3]	Baseline	Pre-BEV	**rNTR** (<5 mL to <10 mL)	$P = .058$[a]	$P = .076$[a]	24
				rNTR > median rNTR (>7.5 mL)	***P* = .002**[a]	***P* = .044**[a]	
				rNTR BEV-R (7.1) vs BEV-NR (2.4) (55 rHGG pts)	***P* = .020**[a]	n.s.[a]	28
				rNTR pre-BEV (volumetric continuous variable)	$P = .290$ (HR .99)[c]	$P = .160$ (HR .98)[c]	25
		Early-BEV	4–6 w scan	**rNTR post-BEV** (volumetric continuous variable)	$P = .210$ (HR .99)[c]	$P = .068$ (HR .99)[c]	25
	Increase in tumor-infiltrative area	Baseline	Pre-BEV	**Percentage of tumor-infiltrative volume** within the total nonenhancing FLAIR lesion (14 rGBM pts)	n.s.[d]	N/A	34
		Early-BEV	8 w scan		***P* = .003**[d]	N/A	
		Late-BEV	16 w scan		***P* = .001**[d]	N/A	

Abbreviations: BEV, bevacizumab; CR, complete response; PR, partial response; w, week; rAG, recurrent anaplastic glioma; HR, hazard ratio; pts, patients; n.s., nonsignificant; N/A, not available.

[1]Enhancing tumor volume (**$V^{CE\text{-}T1WI}$**) = contrast-enhancing tumor on CE-T1WI without necrosis volume.

[2]Edema (**$V^{T2/FLAIR}$**) = area of high T2 or FLAIR-weighted signal intensity (approaching that of cerebrospinal fluid) surrounding the tumor.

[3]Relative nonenhancing tumor ratio (**rNTR**) = ratio of FLAIR volume to CE-T1WI enhancing tumor volume.

[A]*Tumor calcification*, median PFS yes 5.8 m vs no 3.5 m, median OS yes 9.7 m vs no 5.0 m (median detection time 55 d).

[B]*Tumor calcification*, median OS yes 10.5 m vs no 6.6 m. *Tumor calcification + DWI restriction*, median OS yes 13.0 m vs no 6.6 m.

[C]$V^{CE\text{-}T1WI}$*pre-BEV < median* $V^{CE\text{-}T1WI}$ *(19.5 cm*^{3}*)*, median PFS 19.4 m vs 12.0 m, median OS, 60.1 m vs 28.3 m.

[D]$V^{CE\text{-}T1WI}$*post-BEV < median* $V^{CE\text{-}T1WI}$ *(7.8 cm*^{3}*)*, median PFS 20.9 m vs 12.0 m, median OS 64.1 m vs 27.7 m.

[E]$V^{CE\text{-}T1WI}$*post-BEV change (≥ 52% decrease)*, median PFS 24.0 m vs 12.0 m, median OS 52.3 m vs 31.0 m.

[F]$V^{CE\text{-}T1WI}$*post-BEV change (≥ 50% decrease)*, *2D-T1WI*: median OS of patients with vs without progression at 8 and 16 weeks (114 vs 278 days and 214 vs 426 days, $P < .001$); *3D-T1WI*: median OS of patients with vs without progression at 8 and 16 weeks (117 vs 306 d and 223 vs 448 d, $P < .001$).

[a]Log rank test (LR), [b]Cox proportional hazards model (COX, univariable), [c]Cox proportional hazards model (COX, multivariable), [d]Pearson correlation.

in the extracellular space. Restricted diffusion is quantitatively measured by the apparent diffusion coefficient (ADC) value, which is lower in highly cellular tumors and higher in edema and necrosis.[35] Gupta et al[36] reported that decreased ADC might even precede contrast enhancement in progressive HGGs. However, DWI signal changes can be ambiguous and DWI restriction is also found in other pathologies (eg, abscesses, hematomas). In the context of bevacizumab treatment, strokelike diffusion restriction (ie, decreased ADC values) appears shortly (4–8 wk) after treatment initiation and remains stable during treatment course (Fig. 1A).[26,37,38] Histological evaluation of these MRI lesions revealed extensive calcified atypical eosinophilic coagulative necrosis, hyalinization of blood vessels, reactive astrocytosis/gliosis, and increased cellularity, possibly due to infiltration of lymphocytes and monocytes, a phenomenon closely related to the biology of HGG.[26,27,38,39] DWI restriction, especially in combination with tumor calcification on precontrast T1WI, was in most cases related to improved outcome and prolonged response (Tables 1 and 2).[46,58] Therefore, this phenomenon might be used as an early imaging biomarker of treatment response.

ADC values may be able to identify patients with rHGG having a higher chance to benefit from bevacizumab early in therapy or before starting treatment.[40,41] ADC histograms from areas of enhancing tumor were fitted to a mixed model involving a double Gaussian distribution and produced evidence that the mean ADC from the lower curve (ADC_L) was associated with longer PFS and OS during bevacizumab treatment, but not during other chemotherapies.[40–44] Furthermore, the change in the skewed profile of the ADC histogram[45] and a number of MRI parameters derived from functional diffusion maps (fDMs) (traditional vs graded fDMs; linear vs nonlinear fDMs; cell invasion, motility, and proliferation level estimate image maps)[46–48] may be predictive for treatment response early in the course of antiangiogenic therapy (Table 2). In contrast, a decrease in ADC upon treatment in the enhancing and nonenhancing tumor volume appears to be associated with tumor progression, possibly indicating viable and denser tumor tissue.[49] Yamasaki and colleagues[50] demonstrated that a high DWI *b*-value ($b = 4000$) can differentiate between a pseudo-response and real tumor progression during bevacizumab treatment. The *b*-value identifies the measurement's sensitivity to diffusion and determines the strength and duration of the diffusion gradients.

Apart from the described biological ambiguities of ADC changes, methodical concerns such as standardization of measurement parameters, artifact minimization, and improvement of spatial resolution still remain unresolved.

Perfusion-Weighted Imaging

Perfusion-weighted imaging (PWI) as a biomarker for response to antiangiogenic drugs has generated significant interest, as it seems to reflect the direct biological response to bevacizumab.

Dynamic susceptibility contrast (DSC) PWI allows generation of maps of relative CBV (rCBV), relative cerebral blood flow (rCBF), and mean transit time. Mean and median CBV and BBB permeability were significantly reduced after a single dose of bevacizumab, indicating normalization of the abnormal tumor vasculature.[51,52] Recently it was shown that in rHGG patients, pre- and posttreatment rCBV maps could predict significantly longer OS (Table 2).[53] Sawlani et al[54] demonstrated that the percentage change in hyperperfusion volume (the fraction of contrast-enhancing tumor with an rCBV above a predetermined threshold of 1.0) was significantly correlated with PFS in rGBM patients. Component analysis of DSC voxels with perfusion characteristics of both arteries and veins (arteriovenous overlap) revealed an improved median OS in bevacizumab-treated rGBM patients with a decrease in arteriovenous overlap volume (Table 2).[55] Interestingly, in an animal model, serial DSC MR acquisition using the iron oxide contrast agent ferumoxytol was more sensitive in detecting true rCBV and tumor progression than gadodiamide, and this was independent of gadodiamide preload or corticosteroid treatment.[56,57]

The main methodical limitation of DSC MRI in monitoring HGGs is attributed to the presence of the BBB, since gadolinium-containing contrast agent outside the vasculature enhances T1 relaxation of tissue water. This T1 effect may counteract the susceptibility induced signal loss in DSC images leading to an underestimation of CBV and thereby reducing the diagnostic accuracy to detect progression of HGGs. Despite intensive efforts, there is still no generally accepted solution for this methodical problem.[58] In this regard, metabolic active tumor volumes were significantly larger in *O*-(2-[^{18}F]-fluoroethyl)-L-tyrosine (^{18}F-FET) PET than in rCBV maps (tumor volume, 24.3 ± 26.5 cm^3 vs 8.9 ± 13.9 cm^3; $P < .001$), the spatial overlap of both imaging parameters was poor (congruence, 11.0%), and mean distance between the local hot spots differed considerably.[59]

Dynamic contrast-enhanced (DCE) PWI allows measurement of K^{trans}, a value determining the rate at which the contrast agent moves from the vasculature to the extracellular space and therefore representing a marker for BBB permeability. In an animal model, a single dose of bevacizumab significantly decreased tumor vasculature permeability.[57] Sorensen et al[60] studied patients with rGBM treated with cediranib, an inhibitor of the VEGF receptor tyrosine kinases, and calculated a "vascular normalization index" by combining K^{trans}, microvessel volume, and circulating collagen IV measured 1 day after treatment initiation; the authors found this to be predictive of PFS and OS. Again, there are unresolved methodical issues of DCE PWI that reduce the diagnostic accuracy. Parameter calculations of DCE images are based on complex pharmacokinetic compartment models that allow only an approximation of the biological conditions. Other drawbacks of DCE MRI are the low signal change, which results in low signal to noise in the calculated parameter maps, and the large variety of methodical approaches lacking standardization.[61]

MR Spectroscopy

MR spectroscopy (MRS) is the only method that measures intrinsic concentrations of brain metabolites in vivo, giving a greater insight into tumor biology. Proton (^{1}H) spectra of HGGs have a characteristic pattern of metabolite changes that indicate the proliferating activity and cell density of tumor cells (elevated signal intensity of choline-containing compounds [Cho]), as well as the degree of neuronal damage (decreased signal intensity of *N*-acetyl-aspartate [NAA]) and of necrosis (detection of lipid signals).[62] The main drawbacks of ^{1}H-MRS in rHGG are the

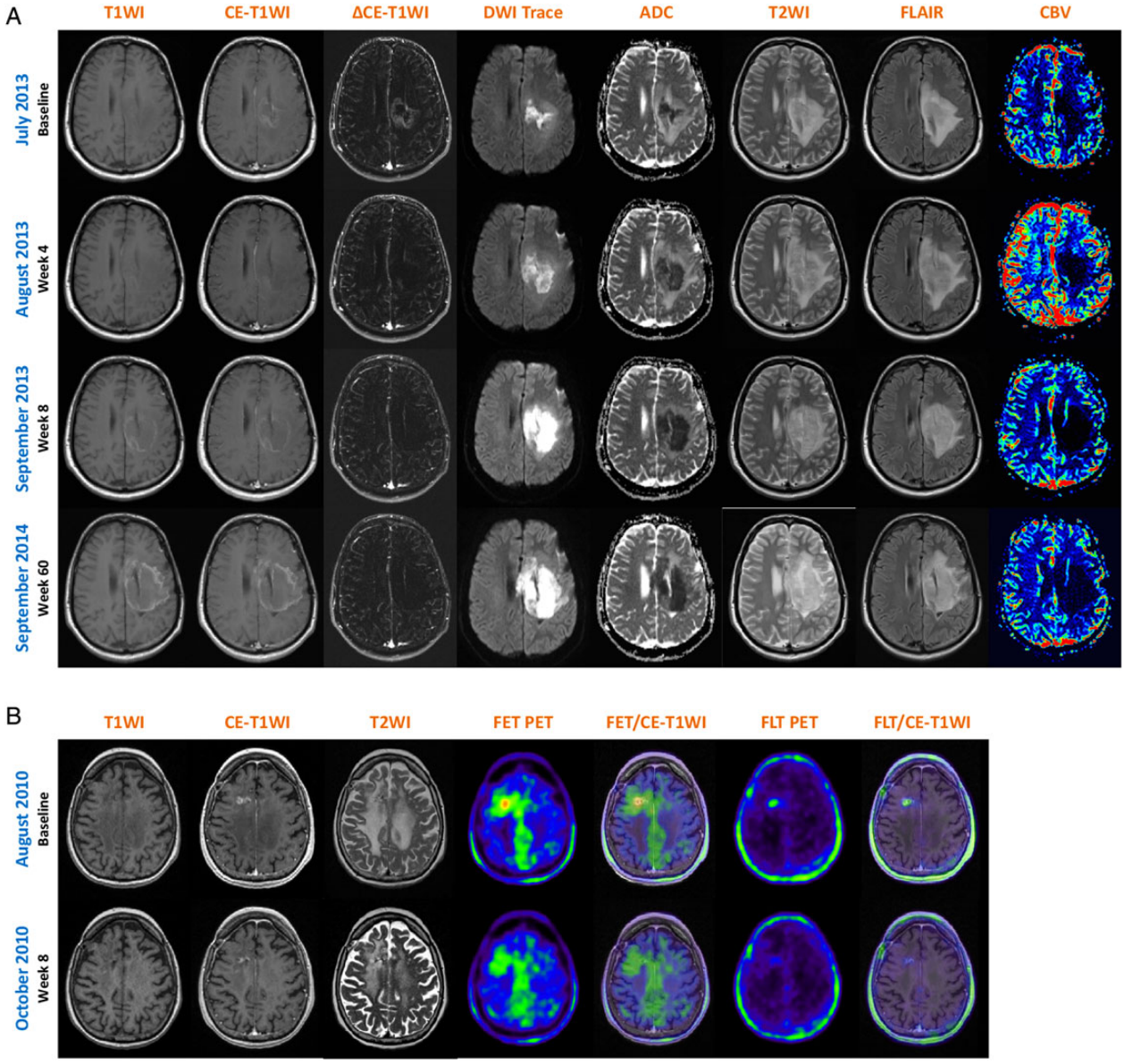

Fig. 1. Representative patients with MRI and PET imaging during antiangiogenic treatment. (A) Baseline and follow-up MRI scans (wk 4, 8, 60) from a male patient with recurrent anaplastic astrocytoma who developed a long-lasting response under bevacizumab treatment (RANO criteria first follow-up scan after 4 wk: no contrast enhancement, significant reduction in T2/FLAIR signal abnormality). The patient developed early (wk 4) hyperintense tumor calcification on precontrast T1WI associated with an extended hypovascularized DWI restriction (low rCBV, high ADC values), indicating calcified coagulative tumor necrosis, blood vessel hyalinization, reactive astrocytosis/gliosis, and increased cellularity due to inflammatory cells. (B) Baseline and first follow-up MRI and ^{18}F-FET/^{18}F-FLT scans from a female patient with recurrent glioblastoma. According to RANO criteria, the patient presented with a partial response due to significant decrease of contrast enhancement and T2/FLAIR signal hyperintensity. At baseline, ^{18}F-FET PET revealed a focal high tracer uptake consistent with the contrast enhancement on MRI, but also a high ratio of nonenhancing metabolically active tumor. The follow-up scan showed a decrease of the focal tracer uptake; the BTV, however, remained stable (metabolic nonresponder). Importantly, ^{18}F-FLT PET demonstrated only tracer uptake dependent on elevated BBB permeability, thereby correlating with MRI contrast enhancement at baseline and the follow-up scan. ΔCE-T1WI = delta T1 map presenting the real contrast enhancement; T2WI = T2-weighted imaging; CBV = relative cerebral blood volume (DSC PWI); FET = ^{18}F-FET PET; FET/CE-T1WI = image fusion of ^{18}F-FET PET and CE-T1WI; FLT = ^{18}F-FLT PET; FLT/CE-T1WI = image fusion of ^{18}F-FLT PET and CE-T1WI.

susceptibility to artifacts, especially in frontotemporal areas near the skull base,[63] and the low signal/noise ratio of metabolite signals. Therefore, enough vital tumor volume without predominant necrosis is needed to discriminate tumor spectra, particularly in rGBM.[64]

Only a few studies investigated MRS during antiangiogenic treatment. Kim and colleagues[63] found an increase in NAA/Cho only 28 days after starting cediranib treatment, suggesting that this antiangiogenic drug has an effect on cellular metabolism that is temporally separated from its immediate

Table 2. Advanced MRI biomarker

Modality	Imaging Biomarker	Time Point	Outcome Measure		Improved PFS	Improved OS	Ref.
DWI	*DWI restriction*[(1)]	Early-BEV	6–8 w scan	**DWI restriction**, 13/18 (72%) HGG pts	N/A	N/A	37
			8–16 w scan	**DWI restriction**, 67/208 (32%) GBM pts	N/A	N/A	36
			8–16 w scan	**DWI restriction**, 35/74 (47%) GBM pts[(A)]	N/A	***P* = .004**[(a)]	26
			8–16 w scan	**DWI restriction**, 20 HGG pts (60 HGG pts, control group)[(B)]	***P* = .013**[(a)]	***P* = .010**[(a)]	38
DWI-ADC	*Mean ADC value*	Early-BEV	8–16 w scan	**Mean ADC value change**, $MRI^{Pre\text{-}BEV\text{-}post1}$	$P = .150$[(a)]	$P = .110$[(a)]	38
			4–6 w scan	**Mean ADC value change**, $MRI^{Pre\text{-}BEV\text{-}post1}$	$P = .790$[(c)]	N/A	41
			3–6 w scan	**Mean ADC value change**, $MRI^{Pre\text{-}BEV\text{-}post1}$	n.s.	n.s.	44
	ADC histograms	Baseline	Pre-BEV	$\mathbf{ADC^{CE\text{-}T1WI} < 1370}$ (mean), (41 rGBM pts)	$P = .140$ (HR 2.1)[(c)]	N/A	41
				$\mathbf{ADC_L^{CE\text{-}T1WI(2)} < 1200}$ (mean)	***P* = .004 (HR 5.5)**[(c)]	N/A	
				$\mathbf{LCP^{CE\text{-}T1WI} > 0.68}$ (mean)	***P* = .010 (HR 3.7)**[(c)]	N/A	
				$\mathbf{ADC^{CE\text{-}T1WI} > 1370}$ (mean)[(D)]	$P = .080$[(a)]	N/A	
				$\mathbf{ADC_L^{CE\text{-}T1WI(2)} > 1200}$ (mean)[(D)]	***P* = .007**[(a)]	N/A	
				$\mathbf{ADC_L^{CE\text{-}T1WI(2)} > mean + LCP^{CE\text{-}T1WI(2)} > mean}$[(D)]	***P* < .001**[(a)]	N/A	
			Pre-BEV	$\mathbf{ADC_L^{CE\text{-}T1WI(2)} < 1209}$ (mean), (91 rGBM pts)	***P* = .008 (OR 2.9)**[(b)]	N/A	43
				$\mathbf{ADC_L^{CE\text{-}T1WI(2)} < mean + LCP^{CE\text{-}T1WI(4)} < mean}$	***P* = .002 (OR 3.6)**[(b)]	N/A	
				$\mathbf{ADC_L^{CE\text{-}T1WI(2)} < 1209}$ (mean)	***P* = .002 (HR 2.3)**[(c)]	***P* = .002 (HR 2.4)**[(c)]	
				$\mathbf{LCP^{CE\text{-}T1WI} > 0.71}$ (mean)	$P = .070$[(c)]	$P = .150$[(c)]	
				$\mathbf{ADC_L^{CE\text{-}T1WI(2)} > 1209}$ (mean)[(E)]	***P* = .015**[(a)]	***P* = .027**[(a)]	
				$\mathbf{ADC_L^{CE\text{-}T1WI(2)} > mean + LCP^{CE\text{-}T1WI(2)} > mean}$[(E)]	***P* < .001**[(a)]	***P* = .002**[(a)]	
			Pre-BEV	$\mathbf{\%ADC_L^{CE\text{-}T1WI(3)}}$ (91 rGBM pts)	$P = .062$ (HR 2.9)[(b)]	***P* = .037 (HR 3.8)**[(b)]	44
				$\mathbf{\%ADC_L^{FLAIR(3)}}$	***P* = .007 (HR 2.9)**[(b)]	***P* = .037 (HR 3.8)**[(b)]	
				$\mathbf{\%ADC_H^{CE\text{-}T1WI(3,4)}}$	***P* = .006 (HR 0.2)**[(b)]	***P* = .003 (HR 1.0)**[(b)]	
				$\mathbf{\%ADC_H^{FLAIR(3)}}$	$P = .220$ (HR 0.3)[(b)]	$P = .690$ (HR 0.7)[(b)]	
				$\mathbf{ADC_L/ADC_M^{CE\text{-}T1WI(3)}}$	***P* = .035 (HR 1.1)**[(b)]	$P = .950$ (HR 1.0)[(b)]	
				$\mathbf{ADC_L/ADC_M^{FLAIR(3,4)}}$	***P* = .008 (HR 1.2)**[(b)]	***P* = .014 (HR 1.2)**[(b)]	
		Early-BEV	3-6 w scan	$\mathbf{\%ADC_L^{CE\text{-}T1WI(3,4)}}$	***P* = .010 (HR 7.0)**[(b)]	***P* = .009 (HR 9.9)**[(b)]	44
				$\mathbf{\%ADC_L^{FLAIR(3)}}$	***P* = .022 (HR 5.9)**[(b)]	$P = .093$ (HR 4.3)[(b)]	
				$\mathbf{\%ADC_H^{CE\text{-}T1WI(3)}}$	***P* = .029 (HR 1.7)**[(b)]	$P = .085$ (HR 0.2)[(b)]	
				$\mathbf{\%ADC_H^{FLAIR(3)}}$	***P* = .032 (HR 0.4)**[(b)]	$P = .750$ (HR 0.7)[(b)]	
				$\mathbf{ADC_L/ADC_M^{CE\text{-}T1WI(3)}}$	$P = .410$ (HR 1.0)[(b)]	$P = .710$ (HR 1.0)[(b)]	
				$\mathbf{ADC_L/ADC_M^{FLAIR(3,4)}}$	***P* = .028 (HR 1.0)**[(b)]	***P* = .002 (HR 1.2)**[(b)]	
	Traditional fDMs[(5)]	Early-BEV	6 w scan	**Vol. ADC^{FLAIR} decrease < 13cc** (median) (77 rGBM pts)	N/A	***P* = .003 (HR 1.98)**[(a)]	46
				Vol. $ADC^{CE\text{-}T1WI}$ decrease < 2cc (median)	N/A	***P* = .001 (HR 2.08)**[(a)]	
	Graded fDMs[(6)]	Early-BEV	6 w scan	**Vol. ADC^{FLAIR} decrease < 12cc** (median)	N/A	***P* = .002 (HR 2.01)**[(a)]	
				Vol. $ADC^{CE\text{-}T1WI}$ decrease < 1.5cc (median)	N/A	***P* < .001 (HR 2.68)**[(a)]	
				Higher mode[(7)] of ADC^{FLAIR}	N/A	$P = .172$ (HR 1.39)[(a)]	
				Higher mode[(7)] of $ADC^{CE\text{-}T1WI}$	N/A	***P* < .001 (HR 3.26)**[(a)]	
	Linear fDMs[(8)]	Early-BEV	6 w scan	$\mathbf{\%V_{ADC}^{CE\text{-}T1WI(9)} < median}$ (linear fDMs) (70 rGBM pts)	$P = .106$[(a)]	$P = .123$[(a)]	47
				$\mathbf{\%V_{ADC}^{FLAIR(9)} < median}$ (linear fDMs)	***P* = .002**[(a)]	***P* = .039**[(a)]	
	Nonlinear fDMs[(8)]	Early-BEV	6 w scan	$\mathbf{\%V_{ADC}^{CE\text{-}T1WI(9)} < median}$ (pre-to-post nonlinear fDMs)	$P = .067$[(a)]	$P = .054$[(a)]	
				$\mathbf{\%V_{ADC}^{CE\text{-}T1WI(9)} < median}$ (post-to-pre nonlinear fDMs)	***P* = .017**[(a)]	***P* = .026**[(a)]	
				$\mathbf{\%V_{ADC}^{FLAIR(9)} < median}$ (pre-to-post nonlinear fDMs)	***P* < .001**[(a)]	***P* < .001**[(a)]	
				$\mathbf{\%V_{ADC}^{FLAIR(9)} < median}$ (post-to-pre nonlinear fDMs)	***P* = .017**[(a)]	***P* = .014**[(a)]	
	CIMPLE[10]	Early-BEV	4–6 w scan	**Vol. proliferative tissue <7.26 mL** (mean) (26 rGBM pts)	$P = .336$[(a)]	$P = .057$[(a)]	48
				mean Rho[(11)] < 3.73 1/yr	***P* = .025**[(a)]	***P* = .005**[(a)]	
				max Rho[(11)] < 34.9 1/yr	$P = .371$[(a)]	$P = .146$[(a)]	
				mean migration[(11)] < 30.1 mm/yr	$P = .909$[(a)]	$P = .612$[(a)]	

Perfusion	*DSC*	Early-BEV	6 w scan	**ΔHPV[12]** cutoff rCBV > 1.0, leakage corrected (16 rGBM pts)	***P* = .002** (HR 1.1)[(c)]	N/A	[54]
		Early-BEV	3–8 w scan	**ΔAVOL[13] volume change** (negative) **[(F)]** (23 rGBM pts)	N/A	***P* = .040**[(a)]	[55]
				ΔAVOL[13] volume change (negative) **[(F)]** (32 rHGG pts)	N/A	***P* = .009**[(a)]	
				ΔrCBV	N/A	*P* = .870[(a)]	
		Baseline	Pre-BEV	**stdRCBV$^{Pre\text{-}BEV(14)}$** < 4400 (ROC)**[(G)]** (36 rHGG pts)	*P* = .480[(a)]	***P* = .002**[(a)]	[53]
		Early-BEV	3–6 w scan	**stdRCBV$^{Post1(14)}$** < 4400 (ROC)**[(G)]**	***P* = .001**[(a)]	***P* = .007**[(a)]	
				stdRCBV$^{Pre\text{-}BEV+\ Post1(14)}$ both < 4400 (ROC)**[(G)]**		***P* < .001**[(a)]	
				stdRCBV$^{Pre\text{-}BEV+\ Post1(14)}$ decrease	N/A	*P* = .190[(a)]	

Abbreviations: BEV, bevacizumab; w, week; HR, hazard ratio; OR, odds ratio; pts, patients; n.s., nonsignificant; N/A, not available; ROC, receiver operating characteristic.

[(1)]*DWI restriction* = lesion with high DWI signal and corresponding low ADC values.

[(2)]*ADC_L* = ADC histogram analysis using a 2-mixture normal distribution to provide optimal curve fitting, ADC_L = mean values for the lower peak (10^{-6} mm^2/s), *LCP* = proportion of total ADCs that were attributable to the lower peak (10^{-6} mm^2/s).

[(3)]*ADC_L* = ADC histogram analysis by using a 4-component histogram curve-fitting method, *ADC_L* = mean values for the lower peak (center 1050 10^{-6} mm^2/s), *ADC_M* = *M1 center* 1150 10-6 mm^2/s, *M2 center* 1350 10^{-6} mm^2/s, *ADC_H* = center 1550 10^{-6} mm^2/s; *%ADC_L* (ADC_L area/total area), *%ADC_H* (ADC_H/total area), ADC_L/ADC_M (ADC_L area/ADC_M area).

[(4)]*Italic* = significant in Cox multivariable analysis, baseline $\%ADC_H^{CE\text{-}T1WI}$ <=or> 25%, baseline ADC_L/ADC_M^{FLAIR} <=or> 0.64, Post-BEV $\%ADC_L^{CE\text{-}T1WI}$ <=or> 62%, Post-BEV ADC_L/ADC_M^{FLAIR} <=or> 1.85.

[(5)]*fDMs* = traditional functional diffusion maps with voxelwise subtraction (ADC change) between post- and pretreatment ADC maps using single-threshold 0.4 μm^2/ms.

[(6)]*Graded fDMs* = graded fDMs show voxels with decreased ADC between 0.25 and 0.4 μm^2/ms.

[(7)]*Mode of ADC* = distribution "mode" as a measure of central tendency based on the ADC distributions within the graded fDM classification.

[(8)]*Linear fDMs* = linear image registration of ADC maps from subsequent follow-up times to pretreatment ADC maps. *Nonlinear fDMs* = nonlinear registration scheme.

[(9)]*%V_{ADC}* = fractional volume of tissue with a significant decrease (ADC < 0.4 μm^2/ms) within CE regions or FLAIR hyperintensities.

[(10)]*CIMPLE* = cell invasion, motility, and proliferation level estimate image maps using serial diffusion MRI scans and a solution to a glioma growth model equation, quantifying the level of aggressive malignant behavior.

[(11)]*mean Rho* = group average value of mean proliferation rate; *max Rho* = group average value of the maximum proliferation rate; *mean migration* = group average value of mean cell migration rate.

[(12)]ΔHPV = percent change in hyperperfusion volume, defined as the percentage of voxels within the contrast-enhancing tumor volume of interest in which rCBV values were greater than a predetermined threshold.

[(13)]Independent component analysis separated vasculature into arterial and venous components; *AVOL* = voxels with perfusion characteristics of both arteries and veins (arteriovenous overlap), which is significantly higher than in normal vasculature (*P* < .001).[55]

[(14)]*stdRCBC* = both pre- and posttreatment rCBV maps were corrected for leakage and standardized to a consistent intensity scale (delta-T1 maps).

[(A)]*DWI restriction*, median OS yes 9.4 m vs no 7.0 m (alterations occurred early 8–12 wk after start of BEV and were stable with time).

[(B)]*DWI restriction*, median PFS yes 8.3 m vs no 5.3 m, median OS yes 55.9 m vs no 21.1 days.

[(C)]*ADC_L < 1200 10^{-6} mm^2/s*, median PFS yes 459 days vs no 315 days; median overall survival yes 581 vs no 429 days.

[(D)]mean *ADC > 1370*, mean PFS yes 195 days vs no 112 days; *ADC_L > 1200*, mean PFS yes 231 days vs no 84 days; *ADC_L >1200 and LCP < 0.68*, mean PFS yes 203 days vs no 90 days.

[(E)]*ADC_L > 1209*, mean PFS yes 209 days vs no 122 days, mean OS yes 329 days vs no 280 days; *ADC_L >1209 and LCP < 0.71*, mean PFS yes 196 days vs no 86 days, mean OS yes 329 days vs no 231 days.

[(F)]*negative vs positive ΔAVOL change after BEV*, GBM (*n* = 23): median OS 348 days vs 197 days, HGG (*n* =32): median OS 399 days vs 153 days.

[(G)]*$stdRCBV^{Pre\text{-}BEV}$ < 4400*, median OS 380 days vs 175 days; *$stdRCBV^{Post1}$ < 4400*, median PFS 167 days vs 78 days, and median OS 340 days vs 186 days); *$stdRCBV^{Pre\text{-}BEV+Post1}$ < 4400*, median OS 395 days vs 100 days.

[(a)]Log rank test (LR), [(b)]Cox proportional hazards model (COX, univariable), [(c)]Cox proportional hazards model (COX, multivariable).

antivascular effects. In line with this hypothesis, a relative NAA/Cho increase after this 28-day time window appears to be predictive of 6-month survival in rGBM patients treated with cediranib or bevacizumab in combination with cytotoxic chemotherapy.[63,65] However, these studies revealed phenomena during treatment and failed to provide predictive parameters before the start of treatment.

More specific changes in tumor metabolism can be evaluated using phosphorus (^{31}P) spectra, which measure metabolites of membrane phospholipids, the intracellular pH, and products of oxidative phosphorylation; all of these are involved in tumor metabolism. Preliminary data suggest that ^{31}P-MRS may be predictive for bevacizumab treatment response. In ^{31}P spectra, the choline peak is differentiated into phosphocholine (PCho) and glycerophosphocholine (GPC). In 32 rGBM patients, PCho/GPC before antiangiogenic treatment was only elevated in patients with short survival time. In 14 patients who were monitored over an extended period, PCho/GPC decreased significantly during antiangiogenic treatment and increased during tumor progression.[66]

PET Imaging

Currently, standard MRI is the most important diagnostic tool for assessing brain tumors because of its excellent soft-tissue contrast and multiplanar reconstruction capabilities.[67] However, structural MRI has key limitations in the identification of nonenhancing tumor parts and in the assessment of treatment response (pseudo-progression, pseudo-response) or tumor recurrence.[14] Metabolic imaging using radiolabeled tracers for PET constitutes an innovative class of tumor imaging and may overcome some of the disadvantages of MRI due to its more accurate estimation of size and extension of the metabolically active tumor.[68,69]

At present, the amino acid tracers [^{11}C]-methionine (^{11}C-MET), ^{18}F-FET, and L-3,4-dihydroxy-6-^{18}F-fluoro-phenylalanine (^{18}F-FDOPA) are the most commonly used for examining metabolic activity of brain tumors.[68–71] Amino acid tracers are substrates to the large neutral amino acid transport system that is highly expressed in tumor and vascular cells of glial brain tumors.[71,72] Elevated tracer uptake, presented as a high standard uptake value (SUV), significantly correlates with tumor cell density and proliferation rate as well as microvascular density.[73] Importantly, the amino acid uptake occurs largely independently of regional tumor perfusion and BBB permeability, identifying nonenhancing tumor areas better than standard MRI alone.[74–76] Moreover, a decrease in amino acid metabolism appears to be an early sign of chemotherapy response in low- and high-grade gliomas.[77,78] Therefore, amino acid PET in conjunction with structural MRI may be more reliable in assessing treatment response of antiangiogenic treatments than MRI alone.[74–76]

Recently, 2 studies demonstrated that ^{18}F-FET PET was able to identify additional nonenhancing metabolically highly active tumor lesions with elevated local CBV that did not respond to anti-VEGF bevacizumab treatment and cannot be derived from MRI assessment based upon RANO criteria alone (Table 3).[74,76] In addition, MRI and ^{18}F-FET PET response assessment was discordant in 36%–40% of patients with significant earlier detection of treatment failure by ^{18}F-FET PET (Fig. 1B), resulting in a median treatment benefit of between 9.0 and 10.5 weeks.[74,76] At the time of the first follow-up scan, 4–8 weeks after the start of treatment, a decrease of more than 45% of the metabolically active biological tumor volume (BTV) differentiated metabolic responders (PFS $\geq$6 mo) from nonresponders (PFS <6 mo) with almost 3 times longer median PFS and significantly longer OS for responders (Table 3).[74,76]

A number of ^{18}F-FET PET studies have shown that the evaluation of the ^{18}F-FET tracer kinetics may provide relevant diagnostic information, especially for noninvasive tumor grading.[79,80] With respect to bevacizumab treatment, a prolonged time to peak (TTP) at baseline had a high predictive value, meaning that a slow flooding of the tumor with ^{18}F-FET tracer correlated to an improved outcome. Furthermore, a reduction in the mean tumor-to-brain ratio (TBR_{mean}) of more than 17% at early follow-up and a certain arrangement of TTP and defined tracer kinetic pattern at baseline and follow-up discriminated responders from nonresponders with a sensitivity of 100% and a specificity of 75% (Table 3).[76]

In line with ^{18}F-FET PET, metabolic imaging by ^{18}F-FDOPA PET measuring absolute BTVs at baseline, 2 weeks, and 6 weeks, as well as their changes between these time points, was predictive for PFS and OS with highest hazard ratios for absolute BTV at 2 weeks and BTV changes at 2 and 6 weeks (hazard ratios, 9.05, 2.94, and 4.02, respectively; Table 3).[23] Furthermore, comparing responders by PET and MRI RANO criteria (6 wk scan), 8/24 cases (33%) were diagnosed discrepant and ^{18}F-FDOPA predicted treatment failure significantly earlier than MRI, leading to a median time benefit of 7.2 weeks (range, 2–20 wk) for earlier detection.[23] The evaluation of voxelwise changes in ^{18}F-FDOPA uptake referring to parametric response maps (PRMs) revealed that a voxelwise increase in ^{18}F-FDOPA uptake in areas of pretreatment contrast enhancement on MRI stratified patients for 3-month PFS and 6-month OS. A decrease in tracer uptake was associated with longer PFS and OS, and vice versa. Finally, the volume fraction of increased ^{18}F-FDOPA uptake between the first 2 posttreatment time points discriminated long- and short-term PFS and OS (Table 3).[81]

[^{18}F]-3′-fluoro-3′-deoxy-L-thymidine (^{18}F-FLT) is an [^{18}F]-labeled thymidine analogue that showed a close correlation between uptake and tumor cell proliferation.[82] Two clinical trials examined the predictive value of ^{18}F-FLT PET in patients with rHGG treated with bevacizumab in combination with irinotecan.[23,83] A reduction of ^{18}F-FLT uptake of more than 25% at 6 weeks served as the optimal threshold for response and discriminated responders (47%) from nonresponders (53%) with longer median OS. Metabolic responders survived 3 times longer in comparison with nonresponders (Table 3).[83] ^{18}F-FLT uptake changes at 2 and 6 weeks were more predictive for PFS and OS than MRI responses.[23,83] Multivariate analysis identified a lack of ^{18}F-FLT reduction at 6 weeks as the strongest independent predictor for PFS and OS.[23] However, the major limitation of this tracer is that a BBB breakdown seems to be a prerequisite for ^{18}F-FLT uptake (Fig. 1B), and even HGGs with high proliferation index may be ^{18}F-FLT negative if they lack contrast enhancement on MRI.[84]

In rHGG receiving antiangiogenic bevacizumab treatment, baseline SUV_{max} and TBR_{max} deriving from ^{18}F-fluoro-deoxyglucose (^{18}F-FDG) PET, a radiolabeled glucose analogue, were

powerful independent predictors of both PFS and OS and were also prognostic for treatment response (Table 3).[85] However, ^{18}F-FDG uptake is problematic in the evaluation of HGG, as the normal brain has a high glucose metabolism background.

PET is ideally suited for the visualization of metabolic processes and specific molecules in the brain and tumor. However, this method lacks the spatial resolution of anatomic information offered by MRI. Therefore, the combination of PET and MRI by hybrid PET/MRI technology is highly complementary, and in future, simultaneous PET/MRI data acquisition will allow the addition of kinetic, functional, and molecular/metabolic information for real-time multiparametric functional imaging.

Image Processing and Data Analysis

The aim of image data analysis in the context of response assessment for HGG is the comparison of pre- and posttreatment data to differentiate responders and nonresponders. Depending on response criteria and imaging modality, a large variety of image processing methods have been developed. Major drawbacks of any advanced MRI technique are the lack of standardized acquisition parameters and of postprocessing algorithms for data evaluation. Further, data need time-consuming postprocessing, unless there is standard and easily applicable software. Consequently, the implementation for clinical routine is work intensive, and the diagnostic value of these MR techniques is difficult to validate, especially between different institutions.

Image Processing for MRI-based Data

To assess treatment response, the volume of the tumor has to be evaluated. Tumor segmentation is a challenging task and can be reached by manual tumor delineation,[86] semi-automatic procedures,[87] and fully automatic algorithms.[88] As manual segmentation is highly dependent on the human operator limiting reliability, semi-automatic approaches should be performed as a minimum.[89] Currently, freely available software like ITK-Snap[45,74] (performing an active contour procedure) and 3D Slicer[90] (with a graph-cut approach) are frequently applied. Particularly in the field of MRI, established preprocessing like denoising,[18] skull stripping,[29] and intensity normalization[86,91] are important prior to segmentation.

Having the tumor regions in pre- and posttreatment images delineated, a histogram analysis of the whole tumor volume can characterize tumor growth.[51,92] Histograms have the advantage that small segmentation errors are negligible.[29] Nevertheless, histograms do not account for the heterogeneous treatment response of GBM.[92]

A voxel-by-voxel comparison of pre- and posttreatment MRIs could overcome this drawback. However, the coregistration of all MRI data to a common baseline is mandatory for this approach. Functional diffusion maps based on ADC data,[46,47] as well as PRMs based on rCBV images,[93] have been established recently as biomarkers for treatment response. It is generally accepted to use an affine transformation model and mutual information as a similarity measure for fDMs and PRMs. However, there is no standard procedure available for image coregistration. Registration approaches, such as MIAMI Fuse and the Functional Magnetic Resonance Imaging of the Brain (FMRIB) Linear Image Registration Tool,[47] lack broad acceptance, and detailed parameters are not yet published.

Furthermore, pre- and posttreatment MRI data suffer from a mixture of linear and nonlinear differences. Reasons for the latter are mainly mass effects of growing tumor. The first approaches to overcome the problem of growing tumors, such as the publicly available GLISTR (glioma image segmentation and registration) approach,[91] adjust the registration to an atlas of healthy volunteers adding a tumor model into the optimization procedure. Other approaches have experimented with the nonlinear B-spline-based FMRIB nonlinear image registration tool of the FMRIB Software Library package with sum-of-squares similarity measure.[47] In the future, more research in this field is warranted.

Image Processing for Combined PET/MRI-based Data

To make use of combined PET/MRI-based data, the tumor region within the PET data has to be delineated, and MRI/PET data have to be coregistered to compare the tumor region in both modalities. An established procedure for tumor delineation in PET is the manual selection of nontumorous regions, such as in the contralateral hemisphere, to determine normal SUV_{mean}. Here, an operator located the tumor by defining a reasonable TBR as a fixed value[94] or by visual inspection.[95] The drawback of this procedure is the operator-dependent selection of the normal tissue region of interest, which might influence the resulting tumor boundary. Several semi-automatic approaches for PET tumor segmentation and the impact of user-dependent parameterization have been studied.[96]

Coregistration of MRI/PET data can be done using commercially or freely available tools, such as PMOD,[71] Statistical Parametric Mapping,[97] VINCI,[76] and iPlan.[95] A comprehensive comparison of the different approaches is impossible considering the number of unknown parameters of coregistration and the large variety of tools and solutions.

Conclusions

The search for clinically useful response criteria and imaging biomarkers of treatment response in HGGs is challenging. In our opinion, state-of-the-art imaging in neuro-oncology has to be tightly adapted to the respective treatment situations. Currently, standard antiangiogenic treatment response assessment (RANO criteria)[14] uses strictly anatomic measurements of structural MRI based on contrast-enhancing tumor on T1WI and hyperintense T2/FLAIR changes. Herein, the major problems of the RANO criteria are as follows: (i) contrast enhancement may significantly decrease following BBB normalization, which is not necessarily indicative of a true antitumor effect ("pseudo-response"), leaving HGG tumor burden without abnormal BBB permeability ("nonenhancing tumor"); (ii) T2/FLAIR signal abnormalities reflect not only metabolically active tumor (solid or infiltrative), but also peritumoral edema (also caused by VEGF-mediated enhanced BBB permeability and typically reduced during anti-VEGF treatment) and treatment-related changes (eg, radiation-associated demyelination or leukencephalopathy, perioperative ischemic or inflammatory effects), which makes it difficult to distinguish tumor from

Table 3. Metabolic PET imaging

Tracer	Imaging Biomarker	Time Point	Outcome Measure			Improved PFS	Improved OS	Ref.
^{18}F-FET	*FET response*[1]	Early-BEV	**BTV decrease ≥45%**	5/11 (45%) rHGG pts (retrospective trial)[A]		***P* = .038**[a]	N/A	74
				6/10 (60%) rHGG pts (prospective trial)[B]		***P* = .001**[a]	***P* = .001**[a]	76
	RANO vs FET[4]	Early-BEV	**Discrepant results in 4/11 (37%) and 4/10 (40%) HGG pts**					74,76
	Treatment failure detection	Late-BEV	**FET PET detected treatment failure significantly earlier than MRI** median time benefit 9.0 w (range, 4–14 w) and 10.5 w (range, 6–12 w)					74,76
	BTV	Early-BEV	**BTV_{mean} decrease %**	Identification of **LTS**: mean change LTS −79.2% vs STS −5.5%		N/A	***P* = .010**[d]	76
	TBR_{max}		**TBR_{max} decrease ≥16%**	Identification of **LTS**: SN 83%, SP 75%, AUC 0.667 ± 0.20		N/A	*P* = .394[e]	
	TBR_{mean}		**TBR_{mean} decrease ≥17%**	Identification of **LTS:** SN 83%, SP 100%, AUC 0.917 ± 0.10		N/A	***P* = .033**[e]	
	TTP	Baseline	**TTP**	Differentiation **LTS**/**STS**: SN 100%, SP 100%, AUC 1.0 ± 0.0		N/A	***P* = .011**[e]	76
		Early-BEV	**TTP change**	Differentiation **LTS**/**STS**: SN 50%, SP 50%, AUC 0.25 ± 0.17		N/A	*P* = .201[e]	
	Kinetic pattern[5]	Baseline	**Type 3 pattern**	Identification of **STS**		N/A	***P* = .030**[f]	
		Early-BEV	**Type 1 pattern**	Identification of **LTS**		N/A	***P* = .030**[f]	
	TTP + kinetic pattern[6]	Early-BEV	**TTP + kinetic pattern**	Differentiation **LTS**/**STS**: SN 100%, SP 75%, AUC 0.94 ± 0.08		N/A	***P* = .025**[e]	
^{18}F-FDOPA	*FDOPA response*[2]	Early- BEV	**BTV decrease ≥ 35%**	2 w scan	16/28 (57%) HGG pts (prospective trial)	***P* < .001**[a]	***P* = .001**[a]	99
				6 w scan	17/24 (71%) HGG pts	***P* = .003**[a]	***P* < .001**[a]	
	RANO vs FDOPA[4]	Early-BEV	**Discrepant results in 8/24 (33%) pts (6 w scan)**					
	Treatment failure detection	Late-BEV	**FDOPA PET detected treatment failure significantly earlier than MRI** median time benefit 7.2 w (range, 2–20 w)					
	SUV_{max}, SUV_{mean}	Baseline	**$SUV_{max,\ mean}$ absolute**			n.s.[a]	n.s.[a]	
		Early BEV	**$SUV_{max,\ mean}$ change**	2 w + 6 w scans		n.s.[a]	n.s.[a]	
	BTV	Baseline	**BTV absolute**	–		***P*** = .530 (HR 1.27)[b]	*P* = .090 (HR 1.9)[b]	
		Early-BEV	**BTV absolute ≤18 mL**	2 w scan	17/28 (61%) HGG pts[D]	***P* = .001**[a]	***P* < .001**[a]	
				6 w scan		***P* = .020**[a]	***P* = .030**[a]	
			BTV absolute ≤18 mL	2 w scan		***P* = .004 (HR 3.9)**[b]	***P* < .001 (HR 9.1)**[b]	
				2 w scan		N/A	***P* < .001 (HR 10.7)**[c]	
				6 w scan		***P* = .020 (HR 3.4)**[b]	***P* = .040 (HR 2.8)**[b]	
			BTV change	0–2 w scan		***P* = .002 (HR 4.3)**[b]	***P* = .010 (HR 2.9)**[b]	
				0–6 w scan		***P* = .010 (HR 3.4)**[b]	***P* = .010 (HR 4.0)**[b]	
				0–6 w scan		N/A	***P* = .020 (HR 4.1)**[c]	
	PRM[7]	Early-BEV	**$Vol(+/-)^{pre\text{-}post1}{}_{FDOPA}$**	**>0.35 cc**	shorter PFS (24 HGG pts)	***P* = .016**[a]	*P* = .122[a]	81
			$\%Vol(+)^{pre\text{-}post1}{}_{FDOPA}$	**>2.5%**	shorter PFS	***P* = .012**[a]	n.s.[a]	
			$Vol(+/-)^{pre\text{-}post1}{}_{FDOPA}$	**>15 cc**	improved 3-m PFS: SN 75%, SP 70%, AUC 0.82	***P* = .011**[e]	*P* = .160[e]	
		Late-BEV	**$\%Vol(+)^{post1\text{-}post2}{}_{FDOPA}$**	**>5.7%**	shorter PFS and OS	***P* = .018**[a]	***P* = .011**[a]	81
			$\%Vol(+)^{post1\text{-}post2}{}_{FDOPA}$	**>2.5%**	improved 6-m OS: SN 91%, SP 83%, AUC 0.83	N/A	***P* = .027**[e]	
^{18}F-FLT	*FLT response*[3]	Early-BEV	**SUV_{mean} decrease ≥25%**	10/19 (53%) HGG pts (prospective trial)[E]		N/A	N/A	83
				16/30 (53%) HGG pts (prospective trial)[F]		N/A	N/A	23
				2 w scan		*P* = .061[a]	***P* = .006**[a]	83
				6 w scan		***P* = .001**[a]	***P* = .002**[a]	
			Lack of FLT response	6 w scan		***P* = .001**[a]	N/A	23
						***P* = .001 (HR 5.6)**[C]	N/A	
	SUV_{mean}	All	**SUV_{mean} absolute**	Not predictive of OS at baseline, 2 w and 6 w scans		N/A	n.s.[a]	23,83
		Early-BEV	**$SUV^{pre\text{-}post1}{}_{mean}$**	R 46% ± 14% decrease vs NR 20% ± 52% increase (*P* = .001)		N/A	N/A	23

	PRM[7]	Early-BEV	**%Vol(+/−)$^{pre\text{-}post1}{}_{FLT}$**	**>70%**	improved 3-m PFS: SN 90%, SP 70%, AUC 0.78	***P* = .022**[e]	N/A	[81]
			Vol(−)$^{pre\text{-}post1}{}_{FLT}$	**>2 cc**	improved 3-m PFS: SN 78%, SP 78%, AUC 0.81	***P* = .024**[e]	N/A	
			Vol(+)$^{pre\text{-}post1}{}_{FLT}$	**>0.3cc**	improved 3-m OS: SN 75%, SP 80%, AUC 0.81	N/A	***P* = .039**[e]	
		Late-BEV	**%Vol(+)$^{post1\text{-}post2}{}_{FLT}$**	**>10%**	shorter PFS	***P* = .004**[a]	n.s.[a]	
^{18}F-FDG	SUV_{max}	Baseline	**SUV_{max}**	**>7**	independent predictor of PFS/OS (25 rHGG pts)	***P* = .001 (HR 8.4)**[c]	***P* = .038 (HR 3.3)**[c]	[85]
	TBR_{max}		**TBR_{max}**	**>1.35**	independent predictor of PFS/OS	***P* = .004 (HR 4.6)**[c]	***P* = .001 (HR 6.0)**[c]	

Abbreviations: BEV, bevacizumab; w, week; m, month; HR, hazard ratio; pts, patients; LTS, long-term survivor (PFS>6 mo); STS, short-term survivor (PFS <6 mo); n.s., nonsignificant; N/A, not available; ROC, receiver operating characteristic.

[(1)]^{18}F-FET response, R = responder with reduction of BTV ≥45%, NR = nonresponder with BTV progression or reduction < 45%.

[(2)]^{18}F-FDOPA response, R = responder with reduction of BTV ≥ 35%, NR = nonresponder with BTV progression or reduction < 35%.

[(3)]^{18}F-FLT response, R = responder with reduction of SUV_{mean} ≥ 25% (AUC 0.779; $P = .017$; SN 82% and SP 80%), NR = nonresponder with SUV_{mean} progression or reduction < 25%.

[(4)]Discrepant result = MRI RANO responder (complete/partial) but no ^{18}F-FET responder.

[(5)]Type 1 pattern = constantly increasing ^{18}F-FET uptake, the curve is always ascending with a clear identifiable peak SUV at the end of the dynamic study; type 2 pattern = the maximum peak is reached at a midway point (TTP >20–45 min) followed by a plateau or a slow descent; type 3 pattern = the peak of the curve occurs at an early time point (TTP ≤20 min) followed by a steep decrease.

[(6)]When 2 of 3 criteria are fulfilled: (1) an increase in TTP of ≥10 min between baseline and follow-up; (2) a TTP of ≥25 min at baseline; and (3) a type 1 or 2 kinetic pattern at follow-up.

[(7)]Parametric response maps (PRMs) = evaluation of voxelwise changes in ^{18}F-FDOPA and ^{18}F-FLT PET uptake; Vol(+/−)$^{pre\text{-}post1}$ = total volume of changing voxels in ^{18}F-FDOPA or ^{18}F-FLT PRMs within areas of contrast enhancement before and after BEV treatment; Vol(**−**)$^{pre\text{-}post1}$ = total volume of tissue with decreasing ^{18}F-FDOPA or ^{18}F-FLT uptake within contrast-enhancing regions on PRMs evaluated before and after BEV treatment; Vol(**−**)$^{post1/post2}$ = total volume of voxels with decreasing ^{18}F-FDOPA or ^{18}F-FLT uptake on PRMs between the 2 posttreatment scans; Vol(+)$^{pre\text{-}post1}$ = total volume of tissue with increasing ^{18}F-FDOPA or ^{18}F-FLT uptake within contrast-enhancing regions on PRMs evaluated before and after BEV treatment; %Vol(+)$^{pre\text{-}post1}$ = volume fraction of increasing ^{18}F-FDOPA or ^{18}F-FLT uptake within areas of contrast enhancement before and after BEV treatment; %Vol(+)$^{post1\text{-}post2}$ = volume fraction of increasing ^{18}F-FDOPA or ^{18}F-FLT uptake within areas of contrast enhancement between the 2 posttreatment time points; %Vol(+/**−**)$^{pre\text{-}post1}$ = total volume fraction (percentage of pretreatment enhancing tumor) of changing voxels on ^{18}F-FDOPA or ^{18}F-FLT PRMs evaluated before and after BEV therapy.

[(A)]*BTV^{FET} decrease ≥45%*, median PFS R 10.2 m vs NR 4.1 m ($P = .025$, MWU test), median OS R 11.0 m vs NR 5.9 m ($P = .120$, MWU test).

[(B)]*BTV^{FET} decrease ≥45%*, median PFS R 9.0 m vs NR 3.3 m ($P = .016$, MWU test), median OS R 23.0 m vs NR 3.5 m ($P = .016$, MWU test).

[(C)]*BTV^{FDOPA} decrease ≥35%*, 2 w scan = mean OS R 13.7 m vs NR 7.0 m ($P = .020$, *t*-test), 6 w scan = mean OS R 14.1 m vs NR 7.6 m ($P = .020$, *t*-test).

[(D)]*BTV^{FDOPA} ≤ 18 mL*, 2 w scan = median OS R 12.1 m vs NR 3.5 m ($P < .001$, *t*-test).

[(E)]*SUV_{mean} decrease ≥ 25%*, median OS R 10.8 m vs NR 3.4 m ($P = .003$, *t*-test).

[(F)]*SUV_{mean} decrease ≥ 25%*, median OS R 12.5 m vs NR 3.8 m ($P = .001$, *t*-test).

[(a)]Log rank test (LR), [(b)]Cox proportional hazards model (COX, univariable), [(c)]Cox proportional hazards model (COX, multivariable), [(d)]Mann–Whitney *U*-test (MWU test), [(e)]receiver operating characteristic (ROC) analysis; SN, sensitivity, SP, specificity, AUC, area under the curve, [(f)]chi-squared (χ^2) test.

nonneoplastic signal alterations; (iii) RANO tumor response evaluation is defined by cutoff values based on T1WI contrast enhancement (partial response, decrease >50%; progression, increase ≥25% or new lesion). Corresponding changes on T2/FLAIR sequences are termed only "significant" or "not significant," without substantiating a defined threshold. A more detailed integration of criteria for T2/FLAIR evaluation—as planned for the next version of the criteria—will not completely clear the problem (see point ii). As discussed later, PET imaging could resolve some of these problems. From our point of view, the RANO criteria should further aim at an improved monitoring of the patients' clinical state, including serial predefined neurological examinations, patient-reported outcome analyses,[98] and, if available, repetitive neurocognitive testing.[6,7]

In our view, antiangiogenic treatment monitoring of HGG patients has routinely to include not only the standard MRI sequences pre-/postcontrast T1WI and T2/FLAIR, but also the widely available DWI, ADC, and DSC PWI. As reviewed in detail, a significant reduction of the contrast-enhancing tumor volume in early MRI scans shortly after start of treatment, but not a decrease in the corresponding T2/FLAIR signal abnormalities, was predictive and/or prognostic for bevacizumab treatment (Table 1). Furthermore, bevacizumab-induced tumor calcification on precontrast T1WI and hypovascularized DWI restrictions (decreased rCBF/rCBV, elevated ADC values) represented strong imaging biomarkers for improved treatment outcome and prolonged response (Tables 1 and 2). Importantly, in GBM patients with or without bevacizumab, nonenhancing DWI-restricted and hypervascularized lesions preceded the development of a new enhancing tumor.[36] Thus, DSC PWI including correction for contrast material leakage (Table 2) should routinely be included.

As presented in detail, additional metabolic PET imaging provides an important and valuable addition to standard MRI. In recent years, especially amino acid PET tracers such as ^{18}F-FET, ^{11}C-MET, and (with a smaller foundation in the literature) ^{18}F-FDOPA were clinically validated for brain tumor diagnosis, treatment planning, and monitoring and have already reached a broad acceptance within the neuro-oncological community, with a wide use in dedicated neuro-oncology centers. The advantages of amino acid PET compared with MRI alone are its possibility (i) to identify both contrast-enhancing and nonenhancing metabolically active high-grade tumor independent from BBB permeability with high sensitivity and specificity,[75] and (ii) to discriminate tumor from nontumor-associated signal abnormalities on T2/FLAIR sequences (eg, peritumoral edema, treatment-related changes).[74,76] Considering its BBB independence and additional value in the evaluation of the metabolically active tumor volumes and TBRs, we recommend that amino acid PET should be further implemented in neuro-oncology multimodal imaging, especially in the course of antiangiogenic treatment monitoring and as study endpoint.

^{18}F-FET and ^{18}F-FDOPA have logistical advantages over ^{11}C-MET due to the longer half-life of the ^{18}F label (109 vs 20 min, respectively) and its independence from a local cyclotron. All 3 tracers provide comparable diagnostic information. ^{18}F-FDOPA, however, has the disadvantage of intensive physiological uptake into the brain basal ganglia, leading to difficult tumor delineation in the situation of adjacent tumor localization (eg, insular, temporal, frontal). Importantly, an ^{18}F-FLT tracer uptake is, in contrast to amino acid tracers, significantly dependent on tumor BBB permeability and is thus restricted mainly to contrast-enhancing tumor lesions (Fig. 1B). Therefore, in our view, response assessment of antiangiogenic treatment in HGG based on ^{18}F-FLT PET has to be interpreted with caution.[84]

In addition to its prognostic and predictive value under antiangiogenic therapy, multimodal imaging combining standard and advanced MRI with amino acid PET imaging may have the ability to detect drug susceptibility or resistance prior to morphological changes. Saying this, a more individually tailored medicine is possible, potentially avoiding overtreatment by significantly earlier detection of treatment failure ("pseudoresponse") than with standard MRI alone (Table 3),[74,76,99] resulting in unnecessary side effects and corresponding costs.[100] Furthermore, comparison of the standard RANO criteria with ^{18}F-FET and ^{18}F-FDOPA response assessment demonstrated that 33%–40% of MRI responders were nonresponders in amino acid PET, revealing a high value of potentially false-responsive diagnosed patients by MRI criteria alone (Fig. 1B).[74,76,99]

Furthermore, the integrated view on combined MRI/PET modality showed at baseline a contrast-enhancing tumor on standard MRI smaller than the median tumor volume (Table 1) and a low mean ADC value of the lower peak (ADC_L; Table 2). It also showed that in early MRI/PET follow-up scans (4–8 wk after treatment started), predictive and/or prognostic imaging biomarkers for antiangiogenic treatment were: a significant reduction of the contrast-enhancing tumor volumes (Table 1), a voxelwise ADC volume change between post- and pretreatment ADC fDMs on standard and advanced MRI (Table 2), a significant reduction of BTVs, and TBR_{mean} using amino acid PETs (Table 3). These observations indicate that patients with a small tumor volume at baseline (eg, after tumor resection of the HGG recurrence) and/or with a favorable treatment response resulting in a small (absolute) residual tumor burden in the early MRI/PET scans may represent a subgroup of HGG patients who respond significantly better than others to bevacizumab. However, the number of investigated patients is low at this time, and no broadly accepted and prospectively evaluated standard methods for defining metabolic responders have been invented.[74,76,99] Therefore, a general recommendation cannot be given, and further prospective data from large populations are necessary.

It is important to process all acquired images adequately (which takes time) and to include the raised information in all relevant procedures. State-of-the-art software tools (though not standardized) should ensure advanced multimodal imaging processing as well as a seamless integration in, for instance, biopsy and radiotherapy planning systems. Interdisciplinary approaches are helpful to reach an optimal integration of all imaging, clinical, and histological information for the sake of the patient.

Unfortunately, the clinical utility of most physiological and metabolic imaging techniques remains unproven at this time, and most of the methods lack standardization. Therefore, well-designed large prospective studies are required to show that the presented preliminary findings are robust, accurate, and reproducible and to determine whether the relationship with outcome is predictive. As advances occur in the development of

therapies that target specific biochemical or molecular pathways and alter tumor physiology in potentially predictable ways, the validation of physiological and metabolic imaging biomarkers in adequately designed trials will become increasingly important in the near future.

Funding

This work was not supported by any funding.

Acknowledgments

The authors confirm the originality of this review. The work was not submitted for publication to another journal.

Conflict of interest statement. M.P. is a consultant to Roche Pharma. P.H. has received honoraria from Roche Pharma as a consultant and speaker.

References

1. Stupp R, Mason WP, van den Bent MJ, et al. Radiotherapy plus concomitant and adjuvant temozolomide for glioblastoma. *N Engl J Med*. 2005;352(10):987–996.
2. Wong ET, Hess KR, Gleason MJ, et al. Outcomes and prognostic factors in recurrent glioma patients enrolled onto phase II clinical trials. *J Clin Oncol*. 1999;17(8):2572–2578.
3. Xu T, Chen J, Lu Y, et al. Effects of bevacizumab plus irinotecan on response and survival in patients with recurrent malignant glioma: a systematic review and survival-gain analysis. *BMC Cancer*. 2010;10:252.
4. De Bonis P, Marziali G, Vigo V, et al. Antiangiogenic therapy for high-grade gliomas: current concepts and limitations. *Expert Rev Neurother*. 2013;13(11):1263–1270.
5. Robles Irizarry LHD, Nakano I, Gladson CL, et al. Therapeutic targeting of VEGF in the treatment of glioblastoma. *Expert Opin Ther Targets*. 2012;16(10):973–984.
6. Chinot OL, Wick W, Mason W, et al. Bevacizumab plus radiotherapy-temozolomide for newly diagnosed glioblastoma. *N Engl J Med*. 2014;370(8):709–722.
7. Gilbert MR, Dignam JJ, Armstrong TS, et al. A randomized trial of bevacizumab for newly diagnosed glioblastoma. *N Engl J Med*. 2014;370(8):699–708.
8. Vredenburgh JJ, Desjardins A, Herndon JE 2nd, et al. Phase II trial of bevacizumab and irinotecan in recurrent malignant glioma. *Clin Cancer Res*. 2007;13(4):1253–1259.
9. Vredenburgh JJ, Desjardins A, Herndon JE 2nd, et al. Bevacizumab plus irinotecan in recurrent glioblastoma multiforme. *J Clin Oncol*. 2007;25(30):4722–4729.
10. Friedman HS, Prados MD, Wen PY, et al. Bevacizumab alone and in combination with irinotecan in recurrent glioblastoma. *J Clin Oncol*. 2009;27(28):4733–4740.
11. Kreisl TN, Kim L, Moore K, et al. Phase II trial of single-agent bevacizumab followed by bevacizumab plus irinotecan at tumor progression in recurrent glioblastoma. *J Clin Oncol*. 2009;27(5):740–745.
12. Taal W, Oosterkamp HM, Walenkamp AM, et al. Single-agent bevacizumab or lomustine versus a combination of bevacizumab plus lomustine in patients with recurrent glioblastoma (BELOB trial): a randomised controlled phase 2 trial. *Lancet Oncol*. 2014;15(9):943–953.
13. Macdonald DR, Cascino TL, Schold SC Jr, et al. Response criteria for phase II studies of supratentorial malignant glioma. *J Clin Oncol*. 1990;8(7):1277–1280.
14. Wen PY, Macdonald DR, Reardon DA, et al. Updated response assessment criteria for high-grade gliomas: response assessment in neuro-oncology working group. *J Clin Oncol*. 2010;28(11):1963–1972.
15. Nowosielski M, Wiestler B, Goebel G, et al. Progression types after antiangiogenic therapy are related to outcome in recurrent glioblastoma. *Neurology*. 2014;82(19):1684–1692.
16. Wang MY, Cheng JL, Han YH, et al. Measurement of tumor size in adult glioblastoma: classical cross-sectional criteria on 2D MRI or volumetric criteria on high resolution 3D MRI? *Eur J Radiol*. 2012;81(9):2370–2374.
17. Boxerman JL, Zhang Z, Safriel Y, et al. Early post-bevacizumab progression on contrast-enhanced MRI as a prognostic marker for overall survival in recurrent glioblastoma: results from the ACRIN 6677/RTOG 0625 Central Reader Study. *Neuro Oncol*. 2013;15(7):945–954.
18. Pichler J, Pachinger C, Pelz M, et al. MRI assessment of relapsed glioblastoma during treatment with bevacizumab: volumetric measurement of enhanced and FLAIR lesions for evaluation of response and progression—a pilot study. *Eur J Radiol*. 2013;82(5):e240–e245.
19. Hasselbalch B, Lassen U, Hansen S, et al. Cetuximab, bevacizumab, and irinotecan for patients with primary glioblastoma and progression after radiation therapy and temozolomide: a phase II trial. *Neuro Oncol*. 2010;12(5):508–516.
20. Desjardins A, Reardon DA, Herndon JE 2nd, et al. Bevacizumab plus irinotecan in recurrent WHO grade 3 malignant gliomas. *Clin Cancer Res*. 2008;14(21):7068–7073.
21. Sathornsumetee S, Desjardins A, Vredenburgh JJ, et al. Phase II trial of bevacizumab and erlotinib in patients with recurrent malignant glioma. *Neuro Oncol*. 2010;12(12):1300–1310.
22. Prados M, Cloughesy T, Samant M, et al. Response as a predictor of survival in patients with recurrent glioblastoma treated with bevacizumab. *Neuro Oncol*. 2011;13(1):143–151.
23. Schwarzenberg J, Czernin J, Cloughesy TF, et al. 3′-deoxy-3′-18F-fluorothymidine PET and MRI for early survival predictions in patients with recurrent malignant glioma treated with bevacizumab. *J Nucl Med*. 2012;53(1):29–36.
24. Ellingson BM, Cloughesy TF, Lai A, et al. Quantitative volumetric analysis of conventional MRI response in recurrent glioblastoma treated with bevacizumab. *Neuro Oncol*. 2011;13(4):401–409.
25. Huang RY, Rahman R, Hamdan A, et al. Recurrent glioblastoma: volumetric assessment and stratification of patient survival with early posttreatment magnetic resonance imaging in patients treated with bevacizumab. *Cancer*. 2013;119(19):3479–3488.
26. Bahr O, Harter PN, Weise LM, et al. Sustained focal antitumor activity of bevacizumab in recurrent glioblastoma. *Neurology*. 2014;83(3):227–234.
27. Bahr O, Hattingen E, Rieger J, et al. Bevacizumab-induced tumor calcifications as a surrogate marker of outcome in patients with glioblastoma. *Neuro Oncol*. 2011;13(9):1020–1029.
28. Norden AD, Young GS, Setayesh K, et al. Bevacizumab for recurrent malignant gliomas: efficacy, toxicity, and patterns of recurrence. *Neurology*. 2008;70(10):779–787.

29. Najafi M, Soltanian-Zadeh H, Jafari-Khouzani K, et al. Prediction of glioblastoma multiform response to bevacizumab treatment using multi-parametric MRI. *PLoS One*. 2012;7(1):e29945.
30. Ananthnarayan S, Bahng J, Roring J, et al. Time course of imaging changes of GBM during extended bevacizumab treatment. *J Neurooncol*. 2008;88(3):339–347.
31. Hattingen E, Jurcoane A, Daneshvar K, et al. Quantitative T2 mapping of recurrent glioblastoma under bevacizumab improves monitoring for non-enhancing tumor progression and predicts overall survival. *Neuro Oncol*. 2013;15(10):1395–1404.
32. Pope WB, Hessel C. Response assessment in neuro-oncology criteria: implementation challenges in multicenter neuro-oncology trials. *AJNR Am J Neuroradiol*. 2011;32(5):794–797.
33. Ellingson BM, Cloughesy TF, Lai A, et al. Quantification of edema reduction using differential quantitative T2 (DQT2) relaxometry mapping in recurrent glioblastoma treated with bevacizumab. *J Neurooncol*. 2012;106(1):111–119.
34. Artzi M, Bokstein F, Blumenthal DT, et al. Differentiation between vasogenic-edema versus tumor-infiltrative area in patients with glioblastoma during bevacizumab therapy: a longitudinal MRI study. *Eur J Radiol*. 2014;83(7):1250–1256.
35. Nelson SJ. Assessment of therapeutic response and treatment planning for brain tumors using metabolic and physiological MRI. *NMR Biomed*. 2011;24(6):734–749.
36. Gupta A, Young RJ, Karimi S, et al. Isolated diffusion restriction precedes the development of enhancing tumor in a subset of patients with glioblastoma. *AJNR Am J Neuroradiol*. 2011;32(7):1301–1306.
37. Rieger J, Bahr O, Muller K, et al. Bevacizumab-induced diffusion-restricted lesions in malignant glioma patients. *J Neurooncol*. 2010;99(1):49–56.
38. Mong S, Ellingson BM, Nghiemphu PL, et al. Persistent diffusion-restricted lesions in bevacizumab-treated malignant gliomas are associated with improved survival compared with matched controls. *AJNR Am J Neuroradiol*. 2012;33(9):1763–1770.
39. Farid N, Almeida-Freitas DB, White NS, et al. Combining diffusion and perfusion differentiates tumor from bevacizumab-related imaging abnormality (bria). *J Neurooncol*. 2014;120(3):539–546.
40. Ellingson BM, Sahebjam S, Kim HJ, et al. Pretreatment ADC histogram analysis is a predictive imaging biomarker for bevacizumab treatment but not chemotherapy in recurrent glioblastoma. *AJNR Am J Neuroradiol*. 2014;35(4):673–679.
41. Pope WB, Kim HJ, Huo J, et al. Recurrent glioblastoma multiforme: ADC histogram analysis predicts response to bevacizumab treatment. *Radiology*. 2009;252(1):182–189.
42. Pope WB, Lai A, Mehta R, et al. Apparent diffusion coefficient histogram analysis stratifies progression-free survival in newly diagnosed bevacizumab-treated glioblastoma. *AJNR Am J Neuroradiol*. 2011;32(5):882–889.
43. Pope WB, Qiao XJ, Kim HJ, et al. Apparent diffusion coefficient histogram analysis stratifies progression-free and overall survival in patients with recurrent GBM treated with bevacizumab: a multi-center study. *J Neurooncol*. 2012;108(3):491–498.
44. Rahman R, Hamdan A, Zweifler R, et al. Histogram analysis of apparent diffusion coefficient within enhancing and nonenhancing tumor volumes in recurrent glioblastoma patients treated with bevacizumab. *J Neurooncol*. 2014;119(1):149–158.
45. Nowosielski M, Recheis W, Goebel G, et al. ADC histograms predict response to anti-angiogenic therapy in patients with recurrent high-grade glioma. *Neuroradiology*. 2011;53(4):291–302.
46. Ellingson BM, Cloughesy TF, Lai A, et al. Graded functional diffusion map-defined characteristics of apparent diffusion coefficients predict overall survival in recurrent glioblastoma treated with bevacizumab. *Neuro Oncol*. 2011;13(10):1151–1161.
47. Ellingson BM, Cloughesy TF, Lai A, et al. Nonlinear registration of diffusion-weighted images improves clinical sensitivity of functional diffusion maps in recurrent glioblastoma treated with bevacizumab. *Magn Reson Med*. 2011;67(1):237–245.
48. Ellingson BM, Cloughesy TF, Lai A, et al. Cell invasion, motility, and proliferation level estimate (CIMPLE) maps derived from serial diffusion MR images in recurrent glioblastoma treated with bevacizumab. *J Neurooncol*. 2011;105(1):91–101.
49. Jain R, Scarpace LM, Ellika S, et al. Imaging response criteria for recurrent gliomas treated with bevacizumab: role of diffusion weighted imaging as an imaging biomarker. *J Neurooncol*. 2010;96(3):423–431.
50. Yamasaki F, Kurisu K, Aoki T, et al. Advantages of high b-value diffusion-weighted imaging to diagnose pseudo-responses in patients with recurrent glioma after bevacizumab treatment. *Eur J Radiol*. 2012;81(10):2805–2810.
51. Vidiri A, Pace A, Fabi A, et al. Early perfusion changes in patients with recurrent high-grade brain tumor treated with bevacizumab: preliminary results by a quantitative evaluation. *J Exp Clin Cancer Res*. 2012;31:33.
52. Jain RK. Normalization of tumor vasculature: an emerging concept in antiangiogenic therapy. *Science*. 2005;307(5706):58–62.
53. Schmainda KM, Prah M, Connelly J, et al. Dynamic-susceptibility contrast agent MRI measures of relative cerebral blood volume predict response to bevacizumab in recurrent high-grade glioma. *Neuro Oncol*. 2014;16(6):880–888.
54. Sawlani RN, Raizer J, Horowitz SW, et al. Glioblastoma: a method for predicting response to antiangiogenic chemotherapy by using MR perfusion imaging—pilot study. *Radiology*. 2010;255(2):622–628.
55. LaViolette PS, Cohen AD, Prah MA, et al. Vascular change measured with independent component analysis of dynamic susceptibility contrast MRI predicts bevacizumab response in high-grade glioma. *Neuro Oncol*. 2013;15(4):442–450.
56. Gahramanov S, Muldoon LL, Li X, et al. Improved perfusion MR imaging assessment of intracerebral tumor blood volume and antiangiogenic therapy efficacy in a rat model with ferumoxytol. *Radiology*. 2011;261(3):796–804.
57. Varallyay CG, Muldoon LL, Gahramanov S, et al. Dynamic MRI using iron oxide nanoparticles to assess early vascular effects of antiangiogenic versus corticosteroid treatment in a glioma model. *J Cereb Blood Flow Metab*. 2009;29(4):853–860.
58. Paulson ES, Schmainda KM. Comparison of dynamic susceptibility-weighted contrast-enhanced MR methods: recommendations for measuring relative cerebral blood volume in brain tumors. *Radiology*. 2008;249(2):601–613.
59. Filss CP, Galldiks N, Stoffels G, et al. Comparison of 18F-FET PET and perfusion-weighted MR imaging: a PET/MR imaging hybrid study in patients with brain tumors. *J Nucl Med*. 2014;55(4):540–545.
60. Sorensen AG, Batchelor TT, Zhang WT, et al. A "vascular normalization index" as potential mechanistic biomarker to

predict survival after a single dose of cediranib in recurrent glioblastoma patients. *Cancer Res*. 2009;69(13):5296–5300.

61. Sourbron SP, Buckley DL. Classic models for dynamic contrast-enhanced MRI. *NMR Biomed*. 2013;26(8):1004–1027.
62. McKnight TR. Proton magnetic resonance spectroscopic evaluation of brain tumor metabolism. *Semin Oncol*. 2004; 31(5):605–617.
63. Kim H, Catana C, Ratai EM, et al. Serial magnetic resonance spectroscopy reveals a direct metabolic effect of cediranib in glioblastoma. *Cancer Res*. 2011;71(11):3745–3752.
64. Rock JP, Hearshen D, Scarpace L, et al. Correlations between magnetic resonance spectroscopy and image-guided histopathology, with special attention to radiation necrosis. *Neurosurgery*. 2002;51(4):912–919; discussion 919–920.
65. Ratai EM, Zhang Z, Snyder BS, et al. Magnetic resonance spectroscopy as an early indicator of response to anti-angiogenic therapy in patients with recurrent glioblastoma: RTOG 0625/ACRIN 6677. *Neuro Oncol*. 2013; 15(7):936–944.
66. Venkatesh HS, Chaumeil MM, Ward CS, et al. Reduced phosphocholine and hyperpolarized lactate provide magnetic resonance biomarkers of PI3 K/Akt/mTOR inhibition in glioblastoma. *Neuro Oncol*. 2012;14(3):315–325.
67. Chen W. Clinical applications of PET in brain tumors. *J Nucl Med*. 2007;48(9):1468–1481.
68. Dunet V, Rossier C, Buck A, et al. Performance of 18F-fluoro-ethyl-tyrosine (18F-FET) PET for the differential diagnosis of primary brain tumor: a systematic review and metaanalysis. *J Nucl Med*. 2012;53(2):207–214.
69. Nihashi T, Dahabreh IJ, Terasawa T. PET in the clinical management of glioma: evidence map. *AJR Am J Roentgenol*. 2013;200(6):W654–W660.
70. Glaudemans AW, Enting RH, Heesters MA, et al. Value of 11C-methionine PET in imaging brain tumours and metastases. *Eur J Nucl Med Mol Imaging*. 2013;40(4):615–635.
71. Kratochwil C, Combs SE, Leotta K, et al. Intra-individual comparison of 18F-FET and 18F-DOPA in PET imaging of recurrent brain tumors. *Neuro Oncol*. 2014;16(3):434–440.
72. Lahoutte T, Caveliers V, Camargo SM, et al. SPECT and PET amino acid tracer influx via system L (h4F2hc-hLAT1) and its transstimulation. *J Nucl Med*. 2004;45(9):1591–1596.
73. Stockhammer F, Plotkin M, Amthauer H, et al. Correlation of F-18-fluoro-ethyl-tyrosin uptake with vascular and cell density in non-contrast-enhancing gliomas. *J Neurooncol*. 2008;88(2): 205–210.
74. Hutterer M, Nowosielski M, Putzer D, et al. O-(2–18F-fluoroethyl)-L-tyrosine PET predicts failure of antiangiogenic treatment in patients with recurrent high-grade glioma. *J Nucl Med*. 2011; 52(6):856–864.
75. Hutterer M, Nowosielski M, Putzer D, et al. [18F]-fluoro-ethyl-L-tyrosine PET: a valuable diagnostic tool in neuro-oncology, but not all that glitters is glioma. *Neuro Oncol*. 2013;15(3): 341–351.
76. Galldiks N, Rapp M, Stoffels G, et al. Response assessment of bevacizumab in patients with recurrent malignant glioma using [18F]fluoroethyl-L-tyrosine PET in comparison to MRI. *Eur J Nucl Med Mol Imaging*. 2013;40(1):22–33.
77. Galldiks N, Kracht LW, Burghaus L, et al. Use of 11C-methionine PET to monitor the effects of temozolomide chemotherapy in malignant gliomas. *Eur J Nucl Med Mol Imaging*. 2006;33(5): 516–524.
78. Wyss M, Hofer S, Bruehlmeier M, et al. Early metabolic responses in temozolomide treated low-grade glioma patients. *J Neurooncol*. 2009;95(1):87–93.
79. Popperl G, Kreth FW, Herms J, et al. Analysis of 18F-FET PET for grading of recurrent gliomas: is evaluation of uptake kinetics superior to standard methods? *J Nucl Med*. 2006;47(3):393–403.
80. Kunz M, Thon N, Eigenbrod S, et al. Hot spots in dynamic (18)FET-PET delineate malignant tumor parts within suspected WHO grade II gliomas. *Neuro Oncol*. 2011;13(3):307–316.
81. Harris RJ, Cloughesy TF, Pope WB, et al. 18F-FDOPA and 18F-FLT positron emission tomography parametric response maps predict response in recurrent malignant gliomas treated with bevacizumab. *Neuro Oncol*. 2012;14(8):1079–1089.
82. Chen W, Cloughesy T, Kamdar N, et al. Imaging proliferation in brain tumors with 18F-FLT PET: comparison with 18F-FDG. *J Nucl Med*. 2005;46(6):945–952.
83. Chen W, Delaloye S, Silverman DH, et al. Predicting treatment response of malignant gliomas to bevacizumab and irinotecan by imaging proliferation with [18F] fluorothymidine positron emission tomography: a pilot study. *J Clin Oncol*. 2007;25(30): 4714–4721.
84. Nowosielski M, Difranco MD, Putzer D, et al. An intra-individual comparison of MRI, [18F]-FET and [18F]-FLT PET in patients with high-grade gliomas. *PLoS One*. 2014;9(4):e95830.
85. Colavolpe C, Chinot O, Metellus P, et al. FDG-PET predicts survival in recurrent high-grade gliomas treated with bevacizumab and irinotecan. *Neuro Oncol*. 2012;14(5):649–657.
86. Angelini ED, Delon J, Bah AB, et al. Differential MRI analysis for quantification of low grade glioma growth. *Med Image Anal*. 2012;16(1):114–126.
87. Chow DS, Qi J, Guo X, et al. Semiautomated volumetric measurement on postcontrast MR imaging for analysis of recurrent and residual disease in glioblastoma multiforme. *AJNR Am J Neuroradiol*. 2014;35(3):498–503.
88. Doyle S, Vasseur F, Dojat M, et al. Fully automatic brain tumor segmentation for multiple MR sequences using hidden Markov fields and variational EM. *Procs. NCI-MICCAI BraTS*. 2013;18–22; http://martinos.org/qtim/miccai2013/proc_brats_2013.pdf.
89. Bauer S, Wiest R, Nolte LP, et al. A survey of MRI-based medical image analysis for brain tumor studies. *Phys Med Biol*. 2013; 58(13):R97–R129.
90. Egger J, Kapur T, Fedorov A, et al. GBM volumetry using the 3D Slicer medical image computing platform. *Sci Rep*. 2013;3:1364.
91. Gooya A, Pohl KM, Bilello M, et al. GLISTR: glioma image segmentation and registration. *IEEE Trans Med Imaging*. 2012; 31(10):1941–1954.
92. Lemasson B, Christen T, Tizon X, et al. Assessment of multiparametric MRI in a human glioma model to monitor cytotoxic and anti-angiogenic drug effects. *NMR Biomed*. 2011; 24(5):473–482.
93. Galban CJ, Chenevert TL, Meyer CR, et al. Prospective analysis of parametric response map-derived MRI biomarkers: identification of early and distinct glioma response patterns not predicted by standard radiographic assessment. *Clin Cancer Res*. 2011; 17(14):4751–4760.
94. Pauleit D, Floeth F, Hamacher K, et al. O-(2-[18F]fluoroethyl)-L-tyrosine PET combined with MRI improves the diagnostic assessment of cerebral gliomas. *Brain*. 2005;128:(Pt 3):678–687.

95. Arbizu J, Tejada S, Marti-Climent JM, et al. Quantitative volumetric analysis of gliomas with sequential MRI and (1)(1)C-methionine PET assessment: patterns of integration in therapy planning. *Eur J Nucl Med Mol Imaging*. 2012;39(5): 771–781.

96. Vees H, Senthamizhchelvan S, Miralbell R, et al. Assessment of various strategies for 18F-FET PET-guided delineation of target volumes in high-grade glioma patients. *Eur J Nucl Med Mol Imaging*. 2009;36(2):182–193.

97. Kiebel SJ, Ashburner J, Poline JB, et al. MRI and PET coregistration—a cross validation of statistical parametric mapping and automated image registration. *Neuroimage*. 1997;5(4 Pt 1):271–279.

98. Holzner B, Schauer-Maurer G, Stockhammer G, et al. [Patient reported outcome monitoring using a tablet PC is suitable for measuring quality of life in patients with gliomas]. *Wien Med Wochenschr*. 2011;161(1–2):6–12.

99. Schwarzenberg J, Czernin J, Cloughesy TF, et al. Treatment response evaluation using 18F-FDOPA PET in patients with recurrent malignant glioma on bevacizumab therapy. *Clin Cancer Res*. 2014;20(13):3550–3559.

100. Heinzel A, Muller D, Langen KJ, et al. The use of O-(2–18F-fluoroethyl)-L-tyrosine PET for treatment management of bevacizumab and irinotecan in patients with recurrent high-grade glioma: a cost-effectiveness analysis. *J Nucl Med*. 2013; 54(8):1217–1222.